ORIGINAL RESEARCH COMMUNICATION

# WNT-3A Regulates an Axin1/NRF2 Complex That Regulates Antioxidant Metabolism in Hepatocytes

Patricia Rada,[1–4] Ana I. Rojo,[1–4] Anika Offergeld,[5] Gui Jie Feng,[5] Juan P. Velasco-Martín,[6]
José Manuel González-Sancho,[2,4] Ángela M. Valverde,[2,7] Trevor Dale,[5]
Javier Regadera,[6] and Antonio Cuadrado[1–4]

## Abstract

***Aims:*** Nuclear factor (erythroid-derived 2)-like 2 (NRF2) is a master regulator of oxidant and xenobiotic metabolism, but it is unknown how it is regulated to provide basal expression of this defense system. Here, we studied the putative connection between NRF2 and the canonical WNT pathway, which modulates hepatocyte metabolism. ***Results:*** WNT-3A increased the levels of NRF2 and its transcriptional signature in mouse hepatocytes and HEK293T cells. The use of short interfering RNAs in hepatocytes and mouse embryonic fibroblasts which are deficient in the redox sensor Kelch-like ECH-associated protein 1 (KEAP1) indicated that WNT-3A activates NRF2 in a $\beta$-Catenin- and KEAP1-independent manner. WNT-3A stabilized NRF2 by preventing its GSK-3-dependent phosphorylation and subsequent SCF/$\beta$-TrCP-dependent ubiquitination and proteasomal degradation. Axin1 and NRF2 were physically associated in a protein complex that was regulated by WNT-3A, involving the central region of Axin1 and the Neh4/Neh5 domains of NRF2. Axin1 knockdown increased NRF2 protein levels, while Axin1 stabilization with Tankyrase inhibitors blocked WNT/NRF2 signaling. The relevance of this novel pathway was assessed in mice with a conditional deletion of Axin1 in the liver, which showed upregulation of the NRF2 signature in hepatocytes and disruption of liver zonation of antioxidant metabolism. ***Innovation:*** NRF2 takes part in a protein complex with Axin1 that is regulated by the canonical WNT pathway. This new WNT-NRF2 axis controls the antioxidant metabolism of hepatocytes. ***Conclusion:*** These results uncover the participation of NRF2 in a WNT-regulated signalosome that participates in basal maintenance of hepatic antioxidant metabolism. *Antioxid. Redox Signal.* 22, 555–571.

## Introduction

**T**RANSCRIPTION FACTOR nuclear factor (erythroid-derived 2)-like 2 (NRF2, also known as NFE2L2) controls the expression of about 1% of human genes, which participate in biotransformation reactions, redox status, energetic metabolism, and proteostasis (1, 15, 18, 24, 32, 55). These genes possess a cis-acting regulatory sequence termed antioxidant response element (ARE) (20, 53) and include, among many others, the ones used in this study in connection with oxidant

metabolism (1, 15, 16, 55). Given the relevance of the liver in energetic metabolism and biotransformation reactions, NRF2 has been extensively studied in metabolic adaptation of hepatocytes (25, 42, 57). NRF2 also participates in liver regeneration (3, 17, 27, 52) and promotes compensatory liver hypertrophy after portal vein branch ligation in mice (43).

NRF2 is controlled by a complex array of transcriptional regulators and post-translational modifications that ensure proper transcriptional activity, under basal conditions and under adaptation to environmental changes (15). Most

[1]Centro de Investigación Biomédica en Red sobre Enfermedades Neurodegenerativas (CIBERNED), ISCIII, Madrid, Spain.
[2]Instituto de Investigaciones Biomédicas ''Alberto Sols'' UAM-CSIC, Madrid, Spain.
[3]Instituto de Investigación Sanitaria La Paz (IdiPaz), Madrid, Spain.
[4]Department of Biochemistry, Faculty of Medicine, Autonomous University of Madrid, Madrid, Spain.
[5]Cardiff School of Biosciences, Cardiff, United Kingdom.
[6]Departamento de Anatomía, Histología y Neurociencia Facultad Medicina, Universidad Autonoma de Madrid, Madrid, Spain.
[7]Centro de Investigación Biomédica en Red de Diabetes y Enfermedades Metabólicas Asociadas (CIBERDEM), ISCIII, Madrid, Spain.

## Innovation

We identify a completely novel regulation of nuclear factor (erythroid-derived 2)-like 2 (NRF2) by the canonical WNT signaling pathway that is redox independent and not connected with $\beta$-Catenin. At the mechanistic level, we show for the first time that NRF2 associates with Axin1 in a WNT-3A-regulated signalosome. Here, NRF2 is phosphorylated by GSK-3 and targeted for ubiquitin/proteasome degradation by $\beta$-TrCP. At the functional level, the relevance of this new pathway is demonstrated in mice with a conditional deletion of Axin1 in the liver. Depletion of Axin1 in these mice results in upregulation of the NRF2-dependent antioxidant metabolism most prominently in hepatocytes of the perivenous zone.

studies have focused on the role of the eletrophile and redox sensor Kelch-like ECH-associated protein 1 (KEAP1) to adjust NRF2 protein levels to metabolic demands. KEAP1 interacts with two regions of NRF2 (amino-acid sequences DLG and ETGE) located at the Neh2 N-terminal domain to direct ubiquitination by the Cullin-3/Rbx1 complex and proteasome degradation of NRF2 (8, 26, 51, 56). On eletrophile modification or oxidation of KEAP1, the interaction with NRF2 is disrupted. Then, NRF2 escapes degradation, enters the nucleus, and targets ARE genes to increase the capacity of antioxidant and biotransformation reactions (31, 48). While the KEAP1 regulation elegantly explains how NRF2 levels adjust to metabolic demands, it does not clarify the role of NRF2 under basal homeostatic conditions or when KEAP1 activity is limiting (see Discussion). Moreover, heterozygous deletion in the *Keap1* gene has different effects on the NRF2 transcriptional signatures of the forestomach, intestine, and liver (32), further supporting the existence of other layers of tissue-specific NRF2 regulation.

We have previously reported that glycogen synthase kinase-3 (GSK-3) phosphorylates NRF2 in the Neh6 domain (amino-acid sequence DSGISL) to create a recognition site for the E3 ligase adapter SCF/$\beta$-TrCP (38, 39). This, in turn, leads to ubiquitin-proteasome degradation of NRF2 through a Cullin-1/Rbx1 complex. The two prototypic mechanisms of

regulation of GSK-3/$\beta$-TrCP comprise the insulin and WNT pathways, where GSK-3 is regulated via phosphorylation or protein complex formation, respectively, but the participation of these pathways in NRF2 regulation has been hardly addressed.

Regarding insulin, it has been suggested that the protein tyrosine phosphatase 1B modulates GSK3$\beta$/NRF2 and Insulin-like Growth Factor-1 Receptor signaling pathways in a model of acetaminophen-induced hepatotoxicity (33). Two recent studies showed that loss of a downstream regulator of insulin signaling, the tumor suppressor phosphatase and tensin homolog (PTEN), results in inhibition of GSK-3 and subsequent induction of NRF2, leading to enhanced cholangiocyte expansion in mice (46) and endometrial carcinogenesis in humans (41).

The experimental evidence connecting NRF2 and WNT signaling is even scarcer despite the fact that WNT is instrumental in acquisition and maintenance of the metabolic signatures of hepatocytes (2, 21, 34, 49). In this study, we have analyzed this connection and its relevance in antioxidant metabolism of hepatocytes taking $\beta$-Catenin as a qualified control. In the absence of canonical WNT signaling, $\beta$-Catenin is recruited to a multi-protein complex composed by the scaffold proteins Axin1 and adenomatous polyposis coli and the kinases casein kinase 1 and GSK-3$\beta$ (45). This protein complex phosphorylates $\beta$-Catenin on conserved N-terminal Ser and Thr residues, thereby marking it for recognition by SCF/$\beta$-TrCP and Cullin-1/Rbx1-mediated ubiquitination and proteasomal degradation. WNT binding to its receptors Frizzled and LRP5/6 at the cell surface results in the disassembly of $\beta$-Catenin from the Axin1-GSK-3$\beta$ complex, leading to accumulation of dephosphorylated $\beta$-Catenin, nuclear import, binding to T-cell factor/lymphoid enhancer factor (TCF/LEF), and upregulation of downstream genes (11).

Here, we report that NRF2 participates in the formation of a protein complex with Axin1/GSK-3/$\beta$-TrCP that is disrupted by WNT-3A, a prototypic canonical WNT ligand, and leads to upregulation of the NRF2 transcriptional signature. This new signaling axis is KEAP1 independent and, therefore, controls antioxidant metabolism of hepatocytes under basal eletrophile pressure.

**FIG. 1. WNT-3A induces the NRF2 transcriptional signature**. **(A–E)** mRNA levels of *Axin2*, *Gs*, *Hmox1*, *Nqo1*, and *Gpx1* normalized by *Actb* (coding $\beta$-Actin) levels, after stimulation of mouse hepatocytes with WNT-3A-CM. **(F)** Immunoblots from mouse hepatocytes stimulated with WNT-3A-CM showing NRF2, $\beta$-Catenin, HO-1, and GS levels. GADPH levels were used as a loading control. **(G)** Densitometric quantification of protein levels from representative blots of **(F)**. **(H–K)** Mouse hepatocytes were transfected with specific siRNAs to knock down *Nfe2l2* (coding NRF2) and stimulated with WNT-3A-CM for 6 h. Messenger RNA levels of *Nfe2l2* **(H)**, *Hmox1* **(I)**, *Nqo1* **(J)**, and *Axin2* **(K)** were normalized by *Actb* levels. For **(A–K)**, values are mean ± SEM (*n* = 3). Statistical analysis was performed with one-way ANOVA followed by Newman–Keuls multiple-comparison test. *$p < 0.05$, **$p < 0.01$, and ***$p < 0.001$ *versus* $t = 0$ or control groups. **(L, M)** HEK293T cells were co-transfected with ARE-LUC **(L)** or TOPFlash **(M)** and pTK-Renilla for normalization, plus NRF2$^{\Delta ETGE}$-V5 or $\beta$-Catenin expression vectors, as indicated. Then, cells were treated with Control- or WNT-3A-CM (16 h). Luciferase activity was measured after 24 h from transfection. Values are mean ± SEM (*n* = 3). *$p < 0.05$ and **$p < 0.01$ *versus* control CM, according to a Student's *t*-test. **(N)** HEK293T cells were transfected with NRF2$^{\Delta ETGE}$-V5 or $\beta$-Catenin as indicated, plus HA-GSK-3$\beta^{\Delta 9}$ and Flag-$\beta$-TrCP. After 24 h, cells were treated with MG132 (40 $\mu M$, 3 h). One-fifth of protein lysate was used to control for protein expression as shown in the *upper panels* (input). The rest of the protein lysates were immunoprecipitated with anti-V5 or anti-$\beta$-Catenin or G protein as a control, and immunoblotted as indicated in the *lower panels* (pull down). *Filled arrowheads* point to HA-GSK-3$^{\Delta 9}$, and Flag-$\beta$-TrCP. *Empty arrowheads* point to the heavy chains of the anti-V5 and anti-$\beta$-Catenin antibodies. ANOVA, analysis of variance; ARE, antioxidant response element; CM, conditioned medium; HEK, human embryonic kidney; HO-1, heme oxygenase-1; GSK-3, glycogen synthase kinase-3; NRF2, nuclear factor (erythroid-derived 2)-like 2; siRNA, short interfering RNA.
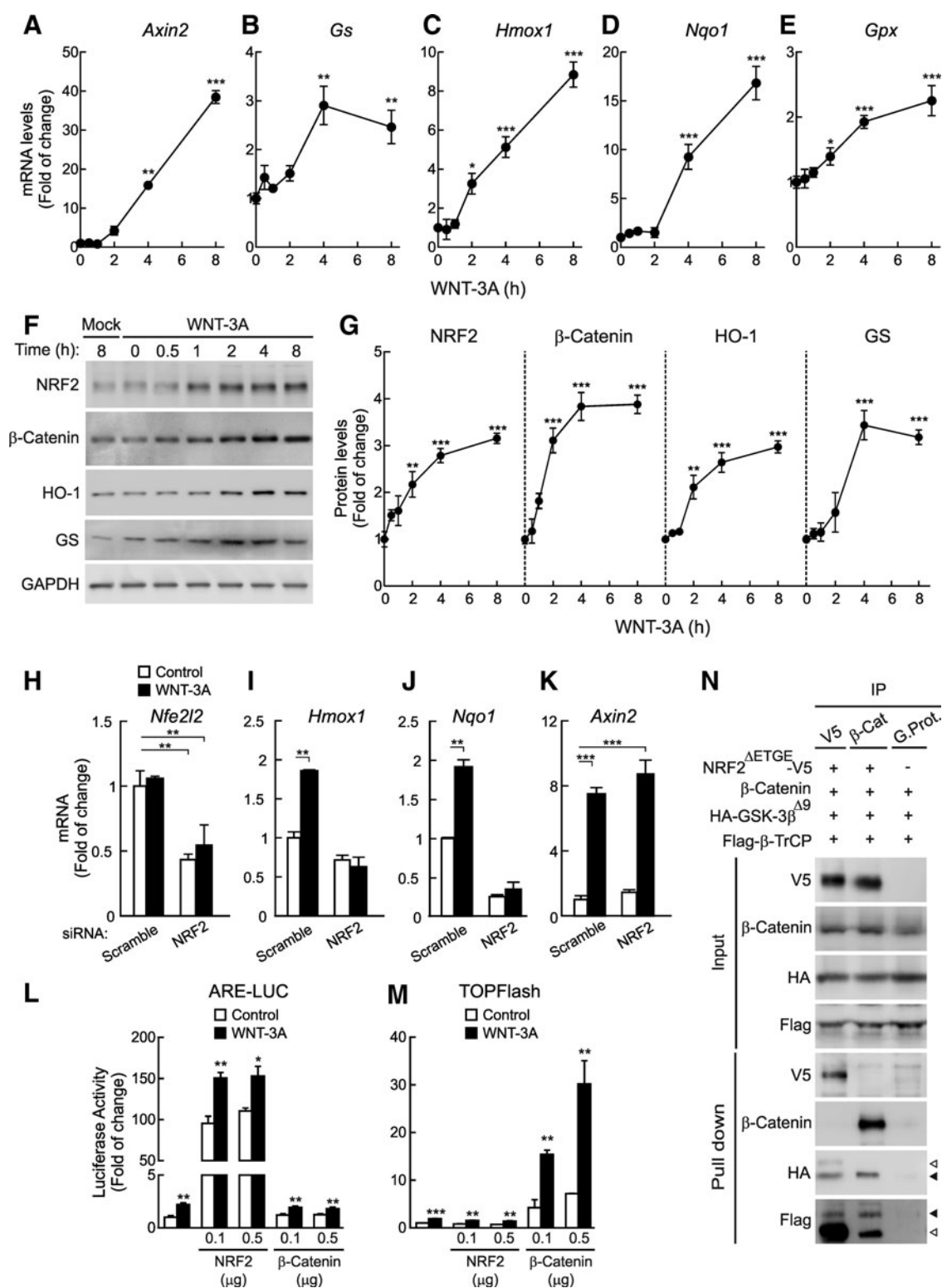
## Results

### The canonical WNT pathway regulates the NRF2/ARE axis

We first analyzed the regulation of NRF2 by WNT-3A. In isolated mouse hepatocytes (Fig. 1A–E), WNT-3A-conditioned medium (CM) (see Materials and Methods) in-duced a time-dependent increase in the messenger RNA levels of two well-established WNT/$\beta$-Catenin targets, *Axin2* and *Gs* (coding glutamine synthetase [GS]), as expected, but, very interestingly, there was a parallel upregulation of genes traditionally considered targets of NRF2, such as *Hmox1* (cod-ing heme oxygenase-1 [HO-1]), *Nqo1* (NAD(P)H:quinone oxidoreductase 1), and *Gpx1* (glutathione peroxidase 1). At
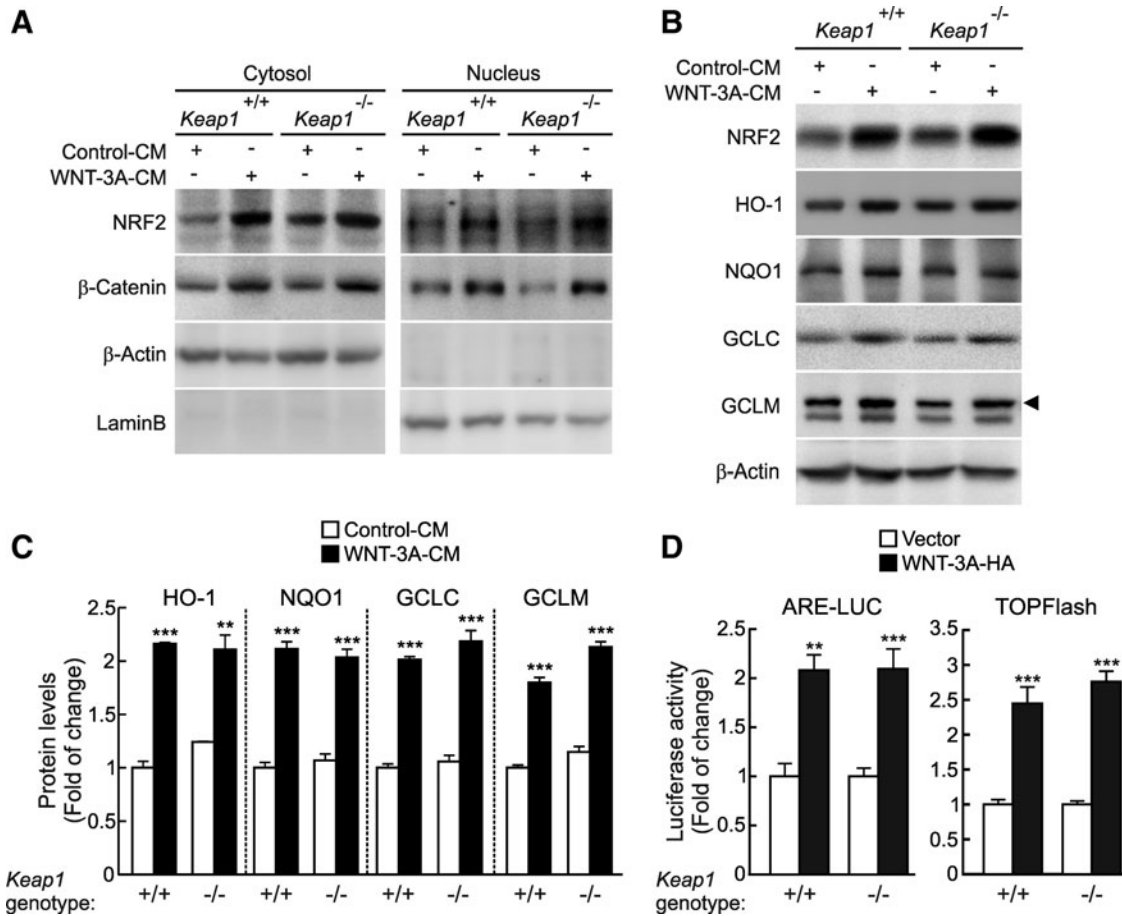
**FIG. 2. WNT-3A increases NRF2 protein levels in a KEAP1-independent manner.** (A) Cytosolic and nuclear extracts from *Keap1*$^{-/-}$ and *Keap1*$^{+/+}$ MEFs treated with control- or WNT-3A-CM for 4 h were immunoblotted with the indicated antibodies. (B) Whole-protein lysates were immunoblotted with the specified antibodies. The *filled arrowhead* points to the band corresponding to GCLM. (C) Densitometric quantification of protein levels from representative blots such as those in (B). Values are mean ± SEM (*n* = 3). \*\**p* < 0.01 and \*\*\**p* < 0.001 *versus Keap1*$^{+/+}$ MEFs treated with control medium, according to a Student's *t*-test. (D) *Keap1*$^{+/+}$ or *Keap1*$^{-/-}$ MEFs were transiently co-transfected with ARE-LUC or TOPFlash reporters, pTK-Renilla, as control, and expression vector for WNT-3A-HA or empty vector. Luciferase activity was measured after 48 h from transfection. Values are mean ± SEM (*n* = 3). \*\**p* < 0.01 and \*\*\**p* < 0.001 *versus* MEFs transfected with empty vector, according to a Student's *t*-test. KEAP1, Kelch-like ECH-associated protein 1; MEFs, mouse embryonic fibroblasts.

**FIG. 3. WNT-3A increases NRF2 protein levels in a GSK-3/β-TrCP-dependent manner.** (A) HEK293T cells were transfected with NRF2-V5. After 24 h, they were further transfected with siRNAs for GSK-3α, GSK-3β, or both or with a control scrambled siRNA. Cells were lysed at 24 h after siRNA transfection. Whole-protein lysates were immunoblotted with specific antibodies as indicated in the panels. (B–E) Mouse hepatocytes were transfected with specific siRNAs to knock down β-*TrCP1* (*Btrc*) and β-*TrCP2* (*Fbxm11*). (B, C) mRNA levels of β-*TrCP1* and β-*TrCP2* after siRNA knockdown. (D, E) mRNA levels of HO-1 and NQO1, respectively, in hepatocytes with specific knockdown of the indicated genes after stimulation with control- or WNT-3A-CM for 6 h. Messenger RNA levels were determined by quantitative real time PCR (qRT-PCR) normalized with β-Actin. Values are mean ± SEM (*n* = 3). Statistical analysis was performed with one-way ANOVA followed by Newman–Keuls multiple-comparison test. \**p* < 0.05, \*\**p* < 0.01, and \*\*\**p* < 0.001 *versus* hepatocytes transfected with scrambled siRNA and treated with control-CM. (F) HEK293T cells were co-transfected with NRF2$^{\Delta ETGE}$-V5 and β-TrCP$^{\Delta Fbox}$-HA. After 24 h, cells were treated with control- or WNT-3A-CM for 3 h. Whole-protein lysates were immunoblotted with specific antibodies as indicated in the panels. (G) HEK293T cells were co-transfected with the NRF2$^{\Delta ETGE}$-V5 or NRF2$^{\Delta ETGE\ 6S6A}$-V5 and His-tagged Ubiquitin. Twenty-four hours after transfection, cells were treated with MG132 for 3 h. Ubiquitinated proteins were isolated in a nickel column, resolved in SDS-PAGE, and immunoblotted with anti-V5 antibody as indicated. Whole-cell lysate (input) and affinity-purified His-tagged fractions (His-Pull down) were blotted with anti-V5 antibody. *Filled and empty arrowheads* point to the positions of NRF2$^{\Delta ETGE}$-V5 and NRF2$^{\Delta ETGE\ 6S6A}$-V5, respectively. The *bracket* indicates the mobility of polyubiquitinated forms of NRF2-V5 (NRF2-Ub).

the protein level, WNT-3A not only increased β-Catenin and GS, but it also led to a comparable increase in NRF2 and HO-1 (Fig. 1F, G). Recombinant WNT-3A also induced a dose-dependent and time-dependent increase in β-Catenin, NRF2, and HO-1 protein levels (Supplementary Fig. S1; Supplementary Data are available online at www.liebertpub .com/ars). These findings correlated with increased NRF2 levels, translocation to the nuclear fraction (Supplementary Fig. S2A), and increased transcriptional activity as determined with an ARE-driven luciferase reporter construct,

ARE-LUC, containing three AREs from the mouse *Hmox1* promoter (Supplementary Fig. S2B, C). Considering that in later experiments we would need to use heterologous expression of NRF2 mutants and WNT signaling proteins, we further validated these observations in human embryonic kidney (HEK) 293T cells that have an intact WNT-3A signaling pathway (29), and we obtained similar outcomes (Supplementary Fig. S3).

To formally demonstrate a role of NRF2 in induction of antioxidant enzymes by WNT-3A, we knocked down *Nrf2*
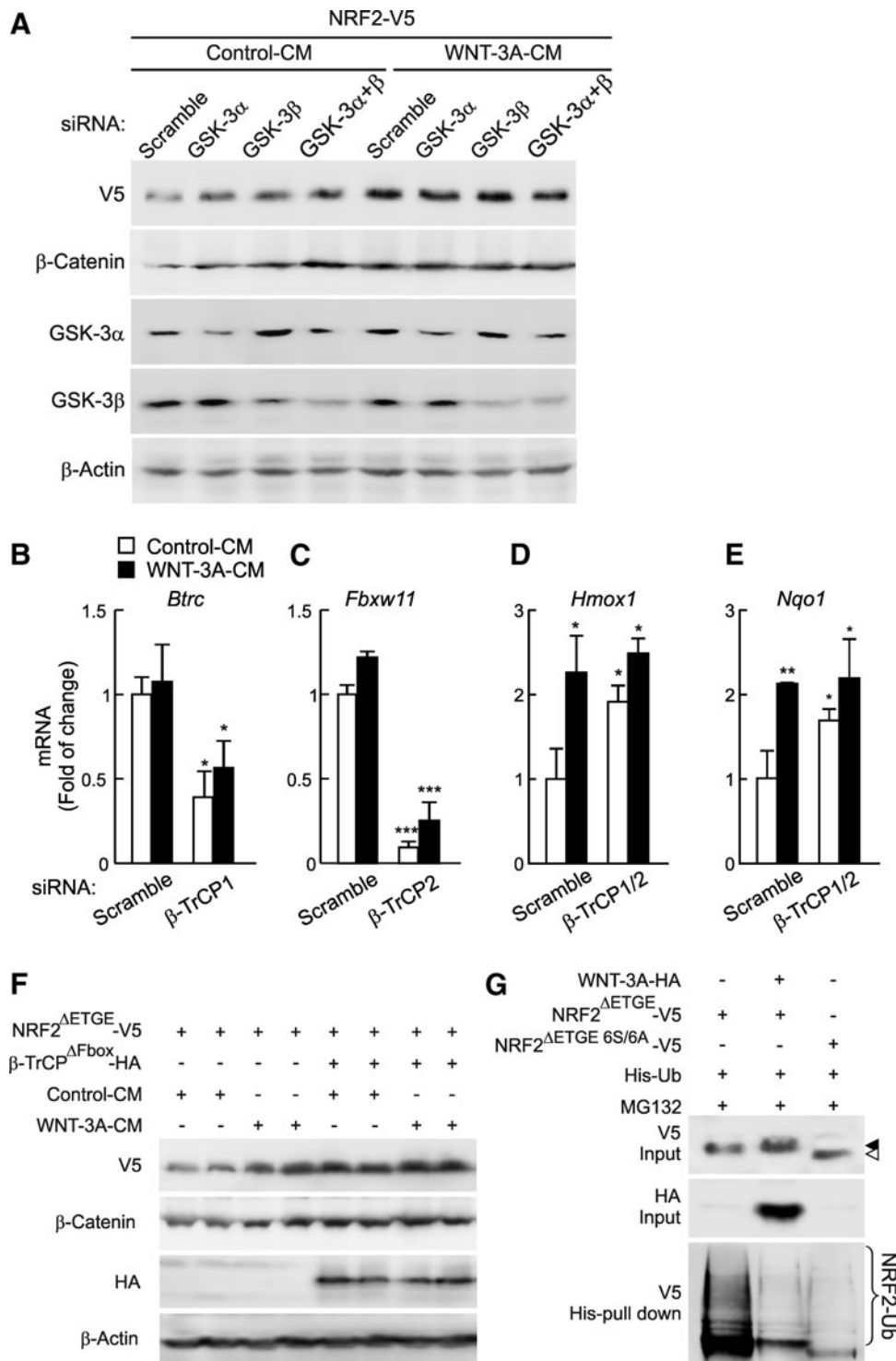
(*Nfe2l2*) expression in mouse hepatocytes with interfering RNA (Fig. 1H–K). Knockdown of *Nrf2* rendered hepatocytes completely unresponsive to WNT-3A-dependent induction of *Hmox1* and *Nqo1*, while *Axin2* expression was unaffected. Altogether, these results demonstrate that the WNT canonical pathway regulates the NRF2/ARE axis.

To further determine whether there might be a functional interference between NRF2 and β-Catenin, we used their respective luciferase reporters ARE-LUC and TOPFlash. HEK293T cells were co-transfected with either of these reporters plus pTK-Renilla as control and different amounts of expression vectors for NRF2$^{\Delta ETGE}$-V5 or β-Catenin. NRF2$^{\Delta ETGE}$-V5 is a stable mutant version of NRF2 with an extended stability, because it lacks the high-affinity binding site for KEAP1 (30, 38, 39). Then, cells were treated with WNT-3A for 16 h. As shown in Figure 1L and M, overexpression of NRF2 but not β-Catenin induced the ARE reporter and WNT-3A led to a similar increase of ARE activity. On the other hand, over-expression of β-Catenin but not NRF2 induced the TOPFlash reporter and WNT-3A led to a similar induction. We also analyzed whether NRF2 and β-Catenin might be a part of a common protein complex. As shown in Figure 1N, immunoprecipitation of either NRF2 or β-Catenin did not pull down the other. As a positive control, we observed that two well-known NRF2 and β-Catenin interacting proteins, GSK-3β and β-TrCP, co-immunoprecipitated with NRF2 or with β-Catenin. Therefore, our results suggest that these two transcription factors are not associated in a common protein complex and that WNT-3A targets them independently.

### WNT regulates NRF2 through a KEAP1-independent but GSK-3/β-TrCP-dependent mechanism

Considering that KEAP1 is the redox-dependent controller of NRF2 stability, we studied whether this E3 ligase adapter might participate in WNT signaling to NRF2 by using mouse embryonic fibroblasts (MEFs) derived from KEAP1-deficient (*Keap1$^{-/-}$*) and wild-type (*Keap1$^{+/+}$*) mice as a control. WNT-3A (4 h) increased the protein levels of NRF2 in wild-type MEFs in both the cytosolic and nuclear fractions in parallel to the increase in β-Catenin used as a control (Fig. 2A). As previously reported, the baseline NRF2 protein levels in *Keap1$^{-/-}$* MEFs were modestly higher than in *Keap1$^{+/+}$* MEFs due to the disruption of KEAP1-mediated degradation of NRF2 (38). However, more relevant, WNT-3A also increased NRF2 levels in *Keap1$^{-/-}$* MEFs. Moreover, on WNT-3A stimulation, we found an induction of approximately two-fold in the NRF2-regulated enzymes HO-1, NQO1, GCLC, and GCLM in both cell lines (Fig. 2B, C). As an alternative approach, we further explored the effect of WNT-3A on the NRF2 transcriptional activity in *Keap1$^{+/+}$* and *Keap1$^{-/-}$* MEFs transfected with the NRF2 luciferase reporter ARE-LUC/pTK-Renilla and the β-Catenin reporter TOP/FOPFlash as control (Fig. 2D). Regardless of the genotype, WNT-3A led to a similar increase in ARE-LUC activity. These results further confirm that WNT-3A stabilizes NRF2 protein levels by a KEAP1-independent mechanism.

Since GSK-3 plays a key role in the WNT signaling pathway, we studied whether GSK-3α or GSK-3β might be involved in the upregulation of NRF2 mediated by WNT-3A. For this purpose, we knocked down each GSK-3 isoform with short

interfering RNAs (siRNAs). HEK293T cells were transfected with an expression vector for NRF2-V5 and then with siRNA against GSK-3α, GSK-3β, or both isoforms (Fig. 3A). Partial knockdown of either protein isoform (about 50%–60% for GSK-3α, and 60%–70% for GSK-3β) was enough to increase NRF2 protein levels, and this effect was maximal when both isoforms were knocked down together. WNT-3A also increased NRF2 protein levels and, in this case, knockdown of GSK-3α, β, or both did not lead to a further effect. A similar effect was observed for β-Catenin, used as a control.

We have previously reported that the E3 ligase adapter SCF/β-TrCP targets NRF2 for proteasome degradation when it had been previously phosphorylated by GSK-3. Therefore, to test the involvement of β-TrCP in the context of WNT signaling to NRF2, we knocked down β-TrCP1 and β-TrCP2 with siRNA in mouse hepatocytes (Fig. 3B–E). Reduction of β-TrCP1/2 levels led to a statistically significant increase in the basal mRNA levels of HO-1 and NQO1, which were close to saturation under WNT-3A induction. This outcome is consistent with a role of this E3 ligase as a negative regulator of NRF2 (7, 38, 39). As an alternative approach, we expressed a dominant-negative mutant (β-TrCP$^{\Delta Fbox}$), which lacks the Fbox motif and cannot form functional complexes with Cullin-1/Rbx1 but competes with endogenous β-TrCP for binding to its substrates (54). To avoid a potential interference with KEAP1, we used the KEAP1-insensitive NRF2 mutant (NRF2$^{\Delta ETGE}$-V5). HEK293T cells were co-transfected with NRF2$^{\Delta ETGE}$-V5 and β-TrCP$^{\Delta Fbox}$-HA, and after 24 h were treated with WNT-3A- or control-CM for 3 h (Fig. 3F). When NRF2 stabilization was achieved by the presence of β-TrCP$^{\Delta Fbox}$, WNT-3A did not promote an additional increase in NRF2, indicating that the inactivation of β-TrCP is involved in the stabilization of NRF2 mediated by WNT-3A. Similar results were found with stabilization of β-Catenin, carried as a control.

Further evidence for the role of WNT-3A in the GSK-3/β-TrCP-mediated regulation of NRF2 was obtained by analyzing the pattern of NRF2 ubiquitination (Fig. 3G). HEK293T cells were co-transfected with plasmids expressing NRF2$^{\Delta ETGE}$-V5, His-Ubiquitin, and either the control vector or an expression plasmid for HA-tagged WNT-3A. Since NRF2$^{\Delta ETGE}$-V5 is not targeted by KEAP1, ubiquitination of this protein rests on other E3 ligase adaptors such as β-TrCP (7, 38, 39). As a control for the GSK-3-independent NRF2-ubiquitination, we also examined the levels of ubiquitinated NRF2$^{\Delta ETGE\ 6S/6A}$-V5, a mutant that is insensitive to both KEAP1 and GSK-3/β-TrCP-mediated degradation pathways (38, 39). WNT-3A led to a significant reduction in the ubiquitination of NRF2$^{\Delta ETGE}$ to levels comparable to those of NRF2$^{\Delta ETGE\ 6S/6A}$, indicating that WNT-3A is blocking NRF2 degradation through the inhibition of GSK-3/β-TrCP pathway. We could still detect residual polyubiquitinated NRF2 in the presence of WNT-3A and in NRF2$^{\Delta ETGE\ 6S/6A}$, indicating the existence of other possible proteasome degradation motifs apart from those involving GSK-3 pathways (7). Taken together, these findings demonstrate that the WNT canonical pathway regulates NRF2 through a mechanism which implies the inhibition of GSK-3/β-TrCP axis.

### Axin1 is involved in the regulation of NRF2

Axin1 is an essential element of the WNT signalosome that scaffolds specific kinases and substrates together (36). To

study the possible connection between NRF2 and Axin1, first we knocked down the expression of Axin1 in $Keap1^{-/-}$ MEFs. In line with the previous data, siRNA-mediated depletion of Axin1 resulted in high NRF2 and $\beta$-Catenin protein levels (Fig. 4A, B). Then, we used two recently characterized small-molecule WNT inhibitors named XAV939 and IWR-1, which inhibit Tankyrase-dependent degradation of Axin1 (6, 19). HEK293T cells were treated for 16 h with vehicle (DMSO), XAV939 (10 $\mu M$), or IWR-1 (20 $\mu M$) and then with WNT-3A-CM for the time points indicated in Figure 4C–E. As expected, Axin1 protein levels were stabilized in HEK293T cells treated with XAV939 or IWR-1. Interestingly, both WNT inhibitors blocked NRF2- as well as $\beta$-Catenin-induction, in response to WNT-3A. Similar results were obtained in mouse hepatocytes (Supplementary Fig. S4). Overall, these data show that genetic inactivation or pharmacologic stabilization of Axin1 inversely modulates NRF2 protein levels.

These results suggested that NRF2 might be a part of a protein complex with Axin1 as is the case for $\beta$-Catenin. To determine whether endogenous NRF2 and Axin1 proteins could be physically associated, we used a co-immunoprecipitation assay in mouse hepatocytes. Cells were treated with MG132 (40 $\mu M$) for 3 h to prevent NRF2 and $\beta$-Catenin degradation and maintain the protein complexes. Both NRF2 and $\beta$-Catenin associated with Axin1 in the same samples (data not shown) and, very importantly, WNT-3A disrupted the Axin1/NRF2 association (Fig. 5A).

Molecular details of Axin1 and NRF2 association were further explored in HEK293T cells. In Figure 5B, KEAP1-insensitive NRF2$^{\Delta ETGE}$-V5 or $\beta$-Catenin, as control, were co-transfected with myc-Axin1, HA-GSK-3$\beta^{\Delta 9}$, and $\beta$-TrCP. Then, cells were maintained in low-serum medium for 16 h and finally treated with WNT-3A. Cellular lysates were immunoprecipitated with anti-V5 for NRF2 or anti-$\beta$-Catenin. In line with the results obtained in hepatocytes, we found that Axin1 interacts not only with NRF2 and $\beta$-Catenin but also with GSK-3$\beta$ and $\beta$-TrCP. Moreover, these interactions were reduced by WNT-3A, suggesting that this factor disassembles the protein complex. Taken together, these data indicate that NRF2 is bound to Axin1 and released from it on WNT-3A stimulation.

### Characterization of the regions of interaction between NRF2 and Axin1

We generated four myc-tagged amino-terminal deletion mutants of mouse Axin1 by consecutive exon deletion
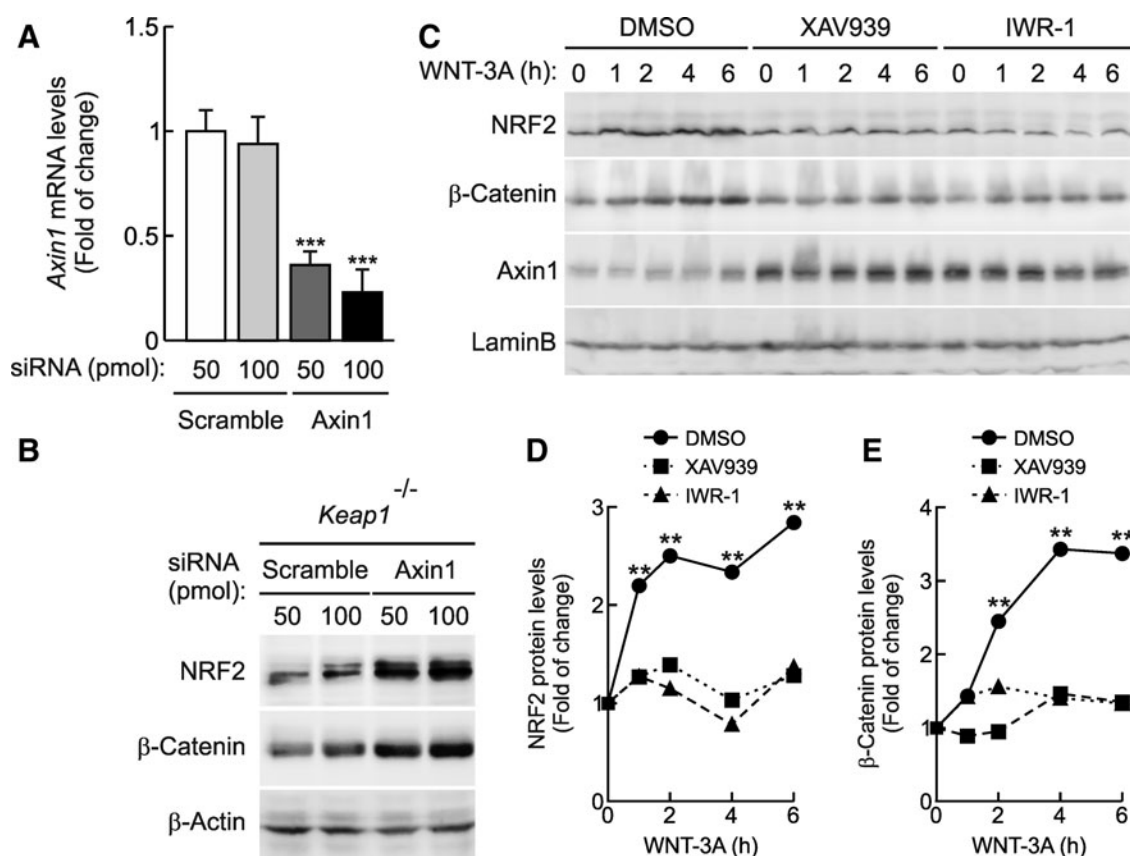


FIG. 4. **Genetic and chemical manipulation of Axin1 alters both WNT/NRF2 and WNT/$\beta$-Catenin signaling. (A)** Messenger RNA levels of *Axin1* normalized by *Actb* in $Keap1^{-/-}$ MEFs transfected with control scrambled or *Axin1* siRNAs. Statistical analysis was performed with a Student's $t$-test. \*\*\*$p < 0.001$ *versus* scramble siRNA. **(B)** Whole-protein lysates of these MEFs were immunoblotted as indicated. **(C)** HEK293T cells were treated with the WNT inhibitors XAV939 (10 $\mu M$) or IWR-1 (20 $\mu M$) or vehicle (DMSO) for 16 h, and then stimulated with WNT-3A-CM according to the indicated time points. Whole-protein lysates were immunoblotted with specific antibodies as indicated in the panels. **(D, E)** Densitometric quantification of NRF2 and $\beta$-Catenin protein levels from representative blots of **(C)**. Statistical analysis was performed with one-way ANOVA followed by Newman–Keuls multiple-comparison test. \*\*$p < 0.01$ *versus* $t = 0$.

from the 3′-end (Fig. 5C). Then, HEK293T cells were co-transfected with these Axin1 deletion mutants and either β-Catenin, as control (Fig. 5E), or NRF2^{ΔETGE}-V5 (Fig. 5F). Co-immunoprecipitation experiments revealed that the Axin1/β-Catenin complex is formed only when exon 6 of Axin1 is present. Regarding NRF2^{ΔETGE}-V5, when cellular lysates were pulled down with anti-V5 antibody, we detected that, similar to β-Catenin, loss of exon 6 resulted in a dramatic reduction of the amount of Axin1 bound to NRF2.

In additional experiments, we determined the region of NRF2 required for Axin1 binding by the use of fusion proteins carrying enhanced yellow fluorescent protein (EYFP) and progressive N-terminal truncations of NRF2, as schematically indicated in Figure 5D. The EYFP-NRF2 chimera Δ1 lacks the Neh2 domain required for binding to KEAP1; it retains the ability to bind Axin1, and this interaction is lost in the presence of WNT-3A (Supplementary Fig. S5). As shown in Figure 5G, immunoprecipitation of NRF2 chimeras revealed that the region comprising the Neh4 and Neh5 domains (*i.e.*, EYFP-NRF2Δ2-V5) is required for binding to Axin1.

*Conditional disruption of Axin1 in the liver results in increased NRF2 transcriptional activity*

We analyzed NRF2 function in the liver of transgenic mice with a conditional liver-specific depletion of Axin1 ($Axin1^{-/-}$) (see Materials and Methods). As shown in Figure 6A and B, these mice showed a dramatic depletion of Axin1. Furthermore, in agreement with (10), total β-Catenin and GS protein levels were not substantially altered. Regarding NRF2, the depletion of Axin1 resulted in upregulation of the NRF2 signature as determined by increased NRF2 protein levels and a two- to four-fold induction of six enzymes regulated by this transcription factor: HO-1, NQO1, GCLC, GCLM, ME1 (malic enzyme 1), and G6PDH (glucose 6 phosphate dehydrogenase). In addition, quantitative real time PCR (qRT-PCR) was used to analyze messenger RNA levels of well-known NRF2 and WNT-specific targets. Levels of Axin1 mRNA were strongly reduced, while there was a modest increase in *Axin2* and *Myc* gene expression and no change in *CyclinD1* and *Gs* (Fig. 6C). This modest increase in β-Catenin-regulated genes is comparable to that reported in the initial characterization of these mice (10) and suggests a compensatory mechanism, maybe mediated in part through *Axin2* upregulation. However, more importantly for our study, with the exception of *Gclc*, mRNA levels of the NRF2-targeted enzymes *Hmox1, Nqo1, Gclm, Gpx, Gsta2, Gstm3*, and *Me1* were increased in $Axin1^{-/-}$ livers (Fig. 6D). These results demonstrate that the basal NRF2 transcriptional signature is inversely dependent on the availability of Axin1 in the liver.

We sought to determine whether $Axin1^{-/-}$ mice show alterations in the phenotypic distribution of enzymes regulated transcriptionally by NRF2. Five-micrometers-thick sections of paraffin-embedded livers were first stained with an anti-NRF2 antibody. Figure 7A shows low and high magnification of NRF2 staining in representative perivenous zones, and Figure 7B shows a negative control in the liver of $Nrf2^{-/-}$ mice. We found that NRF2 was cytosolic and nuclear in $Axin1^{+/+}$ mice. In $Axin1^{-/-}$ mice, NRF2 staining was increased, suggesting not only in agreement with Figure 6 that it was upregulated in the absence of Axin1, but also we counted more hepatocytes with a nuclear accumulation of NRF2 (Fig. 7C). GS distribution was not altered in $Axin1^{-/-}$ livers, as expected (10), indicating that other elements of the WNT pathway may be responsible for regulation of ammonia detoxification (Fig. 7D). However, two enzymes transcriptionally regulated by NRF2, HO-1 (Fig. 7E, G, left panel), and NQO1 (Fig. 7F, G, right panel), which in $Axin1^{+/+}$ livers were expressed around the central vein, exhibited exacerbated expression in the $Axin1^{-/-}$ livers, covering the entire hepatic lobule or expanding toward the periportal zone. Overall, these results demonstrate that the disruption of *Axin1* results in upregulation of NRF2 and its target genes *in vivo* and that NRF2 participates in liver zonation of antioxidant metabolism.

**Discussion**

In this study, we report a completely unexplored link between the canonical WNT-3A signaling pathway and the regulation of antioxidant metabolism by transcription factor

**FIG. 5. Association of NRF2 and Axin1 and disruption by WNT-3A. (A)** Mouse hepatocytes were submitted to control- or WNT-3A-CM for 3 h, as indicated. Input panels show the amount of NRF2 and Axin1 in the protein lysates. NRF2 was immunoprecipitated with anti-NRF2 antibody or G protein as a negative control and analyzed by immunoblot with anti-NRF2 and anti-Axin1 antibodies. **(B)** HEK293T cells were co-transfected with NRF2^{ΔETGE}-V5, or β-Catenin as control, and myc-Axin1, HA-GSK-3β^{Δ9}, and Flag-β-TrCP. After 24 h, cells were treated with control- or WNT-3A-CM in combination with MG132 (40 μM, 3 h). One-fifth of the whole-protein lysate was used to control for protein expression as shown in the *upper panels* (Input). The rest was immunoprecipitated with anti-V5, anti-β-Catenin antibodies, or G protein as a negative control and analyzed by immunoblot with anti-V5, anti-β-Catenin, anti-myc, anti-HA, and anti-Flag antibodies (Pull down). *Filled arrowheads* point to HA-GSK-3^{Δ9} and Flag-β-TrCP. *Empty arrowheads* point to the heavy chains of the anti-V5 and anti-β-Catenin antibodies. **(C)** Diagram showing the exon organization of mouse *Axin1* according to NP_001153070, and the myc-Axin1 chimeras used in pull-down assays with C-terminal deletions of Axin1. The numbers below Axin1 correspond to the amino-acid positions in the boundaries between exons. **(D)** Diagram showing the EYFP-NRF2 chimeras with N-terminal deletions, used to map the region of interaction with Axin1. The numbers below NRF2 correspond to the amino-acid positions in the boundaries between the Neh domains. **(E, F)** HEK293T cells were co-transfected with β-Catenin **(E)** or NRF2^{ΔETGE}-V5 **(F)** and wild-type myc-Axin1 (WT) or the indicated deletion mutants. After 24 h, cells were treated with the proteasome inhibitor MG132 (40 μM, 3 h). One-fifth of whole-protein lysate was used to control for protein expression as shown in the two *upper panels* (input). The rest of the protein lysates were immunoprecipitated with anti-β-Catenin **(E)** or anti-V5 **(F)** and immunoblotted as indicated in the *lower panels*. **(G)** HEK293T cells were co-transfected with myc-Axin1 and EYFP-NRF2 deletion mutants. After 24 h from transfection, cells were treated with the proteasome inhibitor MG132 (40 μM, 3 h). One-fifth of whole-protein lysate was used to control for protein expression as shown in the two *upper panels* (Input). The rest of the protein lysates were immunoprecipitated with anti-V5 and immunoblotted as indicated in the *lower panels*. EYFP, enhanced yellow fluorescent protein. To see this illustration in color, the reader is referred to the web version of this article at www.liebertpub.com/ars

NRF2. Figure 8A describes the elements identified in this new signaling pathway. The canonical WNT pathway has been traditionally connected with development and maintenance of differentiated cell phenotypes, including those of hepatocytes. It is, therefore, very interesting that at least in the liver it exerts a part of this function through the regulation of NRF2. Indeed, while WNT signaling has been demonstrated to regulate antioxidant metabolism through the $\beta$-Catenin-dependent upregulation of some antioxidant genes (13, 35), it is now clear that it also targets the NRF2 signature. This is done in a $\beta$-Catenin-independent manner (Fig. 1), further suggesting that these transcription factors, although regulated by WNT, operate independently.

Most signaling pathways lead to production of reactive oxygen species that might contribute to regulation of NRF2

by interfering with the redox sensor KEAP1. In the case of WNT, a role for this redox modulation was reported through the RAC1 GTPase-dependent activation of NADPH oxidase 1 (NOX1) (22). In addition, the Wilms tumor gene on X chromosome (WTX) inhibits degradation of NRF2 through competitive binding to KEAP1 (5). These observations indicated the importance of determining whether WNT was somehow modulating the KEAP1/NRF2 response. We found that the WNT regulation of NRF2 was independent of KEAP1, because (i) WNT-3A stabilized the KEAP1-insensitive mutant NRF2$^{\Delta\text{ETGE}}$-V5 and (ii) WNT-3A stabilized endogenous NRF2 in MEFs from $Keap1^{-/-}$ mice.

On the other hand, we found that Axin1 binding, GSK-3$\beta$ phosphorylation, and $\beta$-TrCP ubiquitination of NRF2 were disrupted by WNT-3A and, therefore, established the basis to
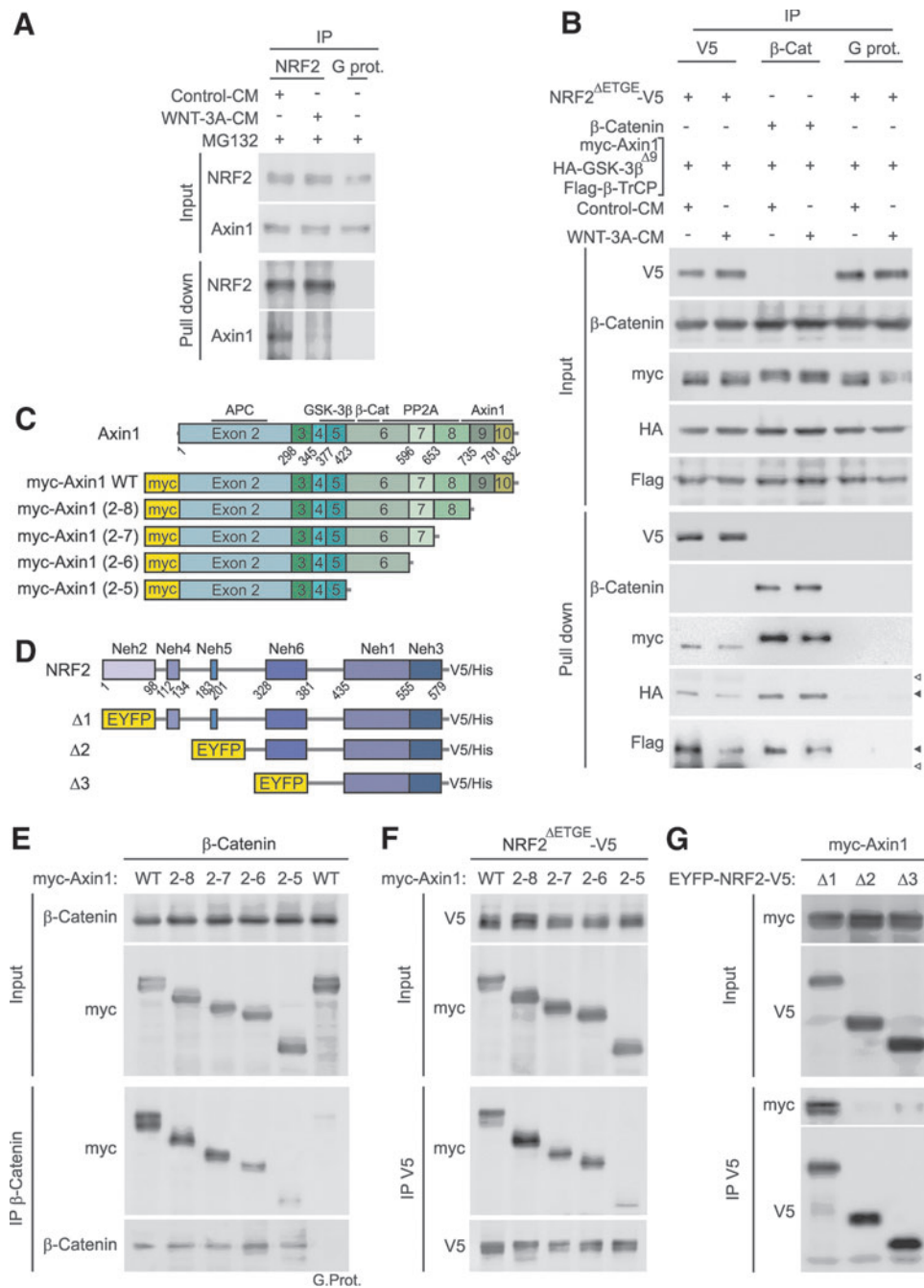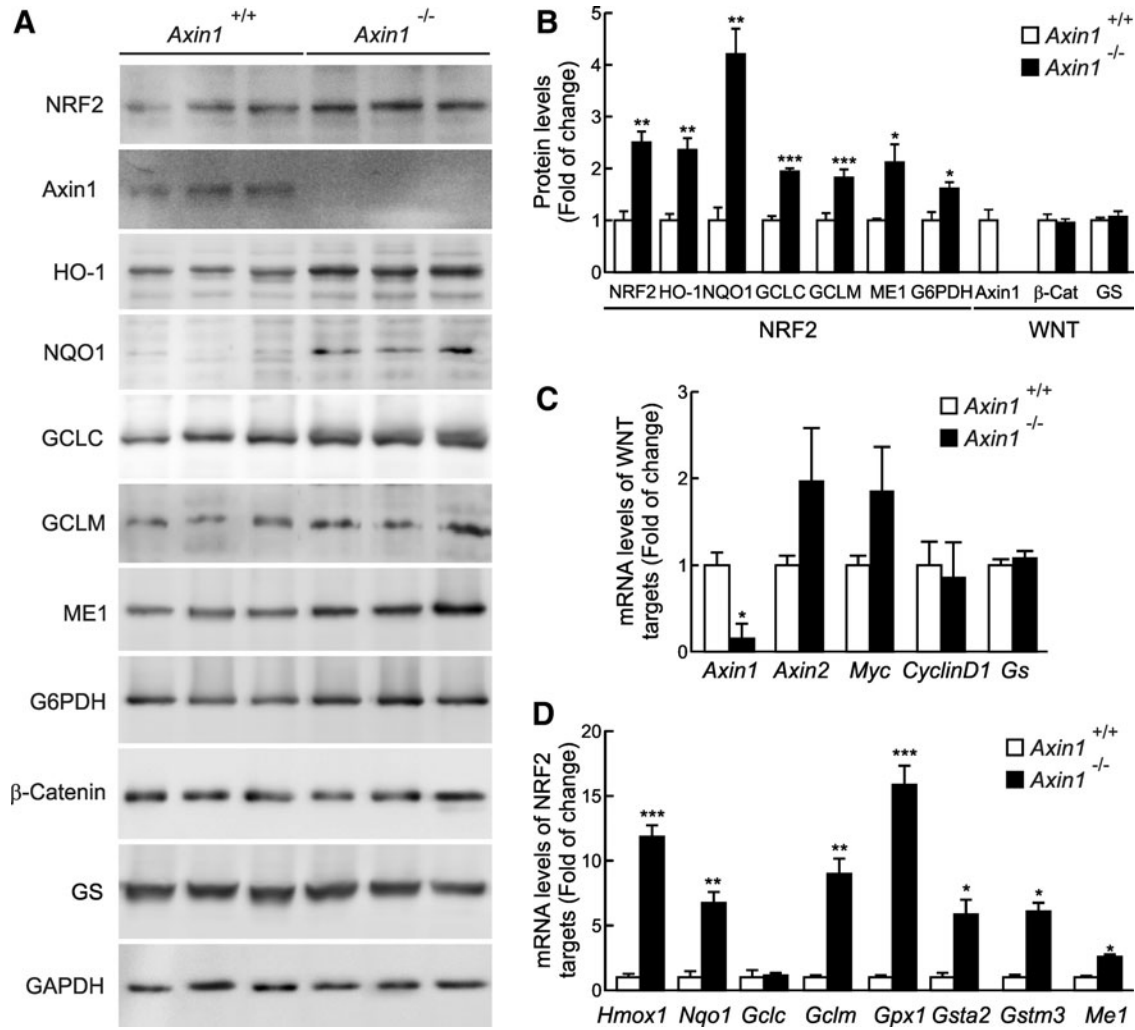
**FIG. 6.   Selective loss of Axin1 in the livers of floxed Axin1$^{-/-}$ mice increased NRF2 signature. (A)** Liver extracts from *Axin1$^{+/+}$* and *Axin1$^{-/-}$* were immunoblotted with the indicated antibodies. Each lane corresponds to liver extracts prepared from different mice. **(B)** Densitometric quantification of protein levels from representative blots of **(A)**. Values are mean ± SEM ($n = 3$). *$p < 0.05$, **$p < 0.01$, and ***$p < 0.001$ *versus Axin1$^{+/+}$* mice according to a Student's *t*-test. **(C)** mRNA levels of *Axin1*, *Axin2*, *Myc*, *CyclinD1*, and *Gs*. Values are mean ± SEM ($n = 3$). *$p < 0.05$ *versus Axin1$^{+/+}$* mice, according to a Student's *t*-test. **(D)** mRNA levels of *Hmox1*, *Nqo1*, *Gclc*, *Gclm*, *Gpx1*, *Gsta2*, *Gstm3*, and *Me1* determined by qRT-PCR and normalized by *β*-Actin. Values are mean ± SEM ($n = 3$). *$p < 0.05$, **$p < 0.01$, and ***$p < 0.001$ *versus Axin1$^{+/+}$* mice according to a Student's *t*-test.

**FIG. 7.   Alteration of Axin1/NRF2 disrupts liver zonation of antioxidant metabolism.** Five-micrometer-thick paraffin sections from the livers of *Axin1$^{+/+}$* and *Axin1$^{-/-}$* mice were stained as indicated. CV, central vein; PV, portal vein. Scale bars = 100 *μ*m. **(A)** NRF2 staining in the perivenous region of a hepatic lobule. **(B)** Negative control for the anti-NRF2 antibody in a section of *Nrf2$^{-/-}$* mouse liver. **(C)** Percentage of NRF2-positive nuclei in the perivenous region of *Axin1$^{+/+}$* and *Axin1$^{-/-}$* mice. The number of cells with NRF2 nuclear staining was counted in fields around the perivenous region. The total number of cells per field was obtained by adding the NRF2 nuclear positive cells and cells with Harris' hematoxylin nuclear staining. Values are mean ± SEM ($n = 6$ fields per genotype). ***$p < 0.001$ *versus Axin1$^{+/+}$* mice, according to a Student's *t*-test. **(D)** Similar zonation of GS in *Axin1$^{+/+}$* and *Axin1$^{-/-}$* livers, as expected from (10). **(E)** HO-1 staining. **(F)** NQO1 staining. *Upper panels* for **(E, F)**; note the increase in HO-1 and NQO1 staining intensity in the *Axin1$^{-/-}$* liver. *Lower panels* for **(E, F)**; note that in *Axin1$^{+/+}$* liver, expression of HO-1 and NQO1 is localized mainly in the hepatocytes closest to the CV, while in *Axin1$^{-/-}$* liver expression of these markers is evident in hepatocytes located at a further distance. **(G)** Densitometric estimation of respective HO-1 and NQO1 staining. Twenty five perivenous regions from five mice were analyzed with a mask of 20 × 20 *μ*m as indicated in Materials and Methods. Values correspond to percentage of specific staining ($n = 25$) broken down by distance to the CV ± SEM. *$p < 0.05$, **$p < 0.01$ according to two-way ANOVA with *post hoc* Bonferroni's test. To see this illustration in color, the reader is referred to the web version of this article at www.liebertpub.com/ars

study this novel mechanism of NRF2 regulation. We mapped the region of interaction between NRF2 and Axin1 to the exon 6 of Axin1. This is a critical scaffolding segment of Axin1, termed the central region, that enables Axin1 to interact with several proteins, including transcription factors $\beta$-Catenin, MYC, Smad3, and p53 as well as protein kinases GSK-3$\beta$, CK1, MKK1, and MKK4, among others (36). This region is natively unfolded, and it has been suggested to undergo a sort of "induced fit" to accommodate specific groups of proteins. Thus, our study suggests that Axin1 scaffolds a complex with NRF2, GSK-3$\beta$, and $\beta$-TrCP to downregulate NRF2. The existence of several proteins

which compete for binding to Axin1 in the same region suggests that Axin1 levels may be limiting to control specific WNT pathways.

In addition to the well-characterized KEAP1/NRF2 system, it is becoming clear that other regulatory mechanisms also operate on NRF2. In fact, graded reduction in expression of *Keap1*, achieved in mouse liver by several genetic techniques, leads to graded increase NRF2 levels (47, 55), suggesting that KEAP1 operates close to saturation and that an increase in NRF2 overloads this mechanism. Formal proof of this hypothesis is lacking, as, to our knowledge, a comparison of turnovers of KEAP1 and NRF2 under different
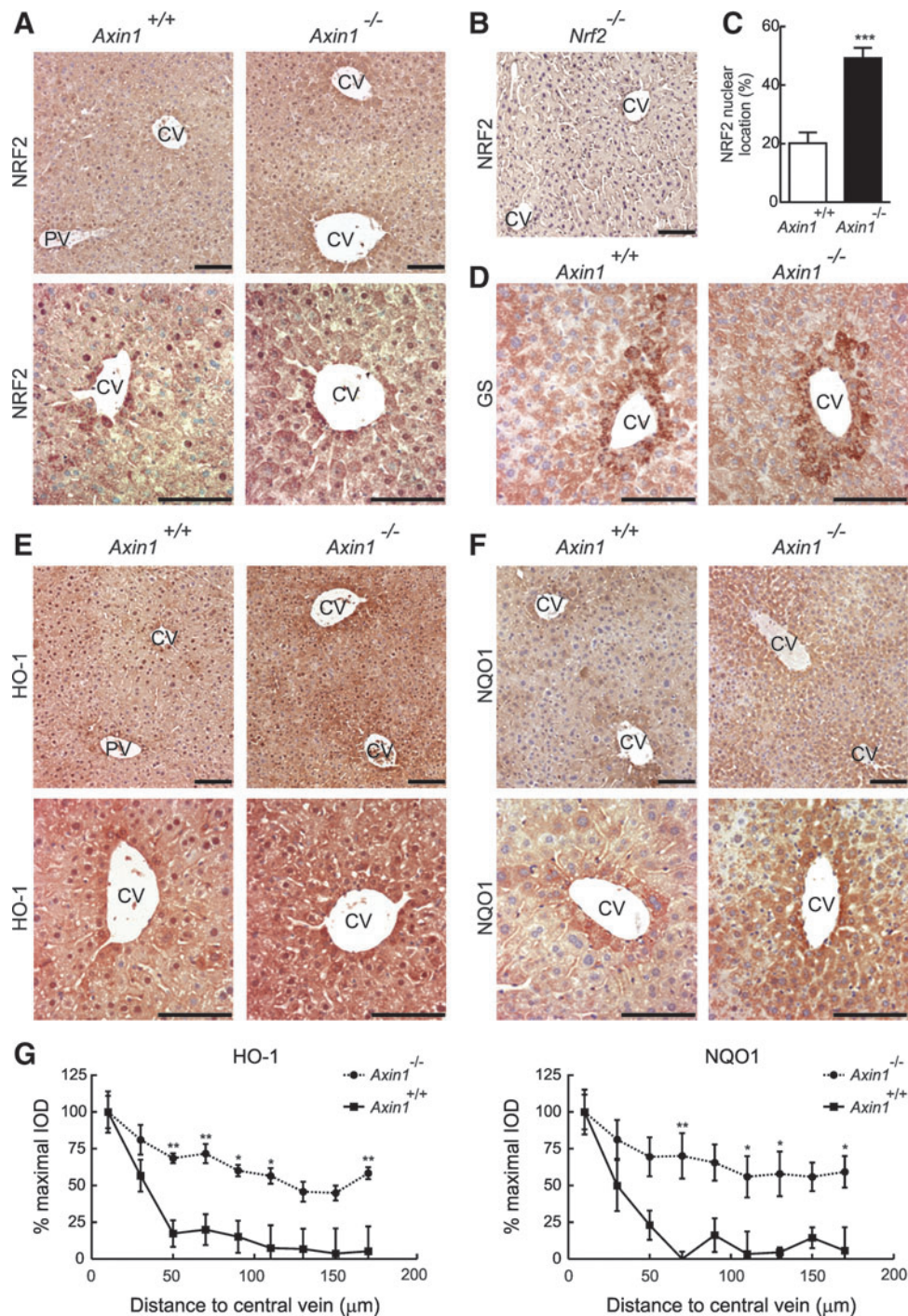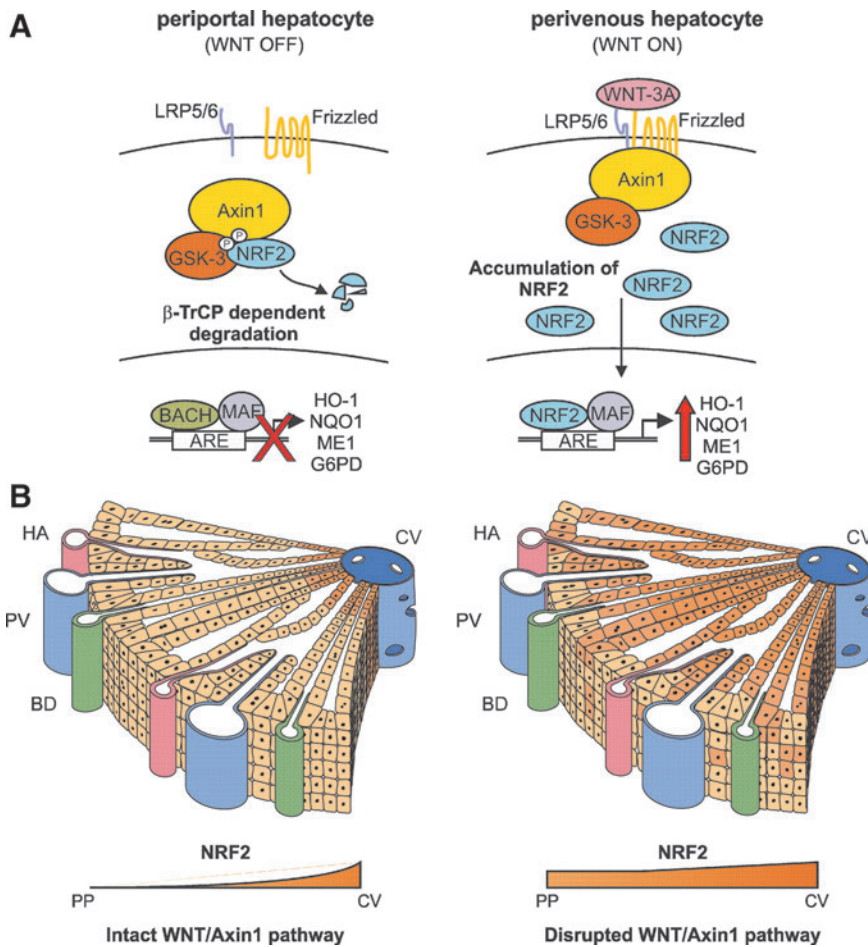
**FIG. 8. Proposed modulation of NRF2 by WNT-3A. (A)** Under unstimulated conditions (WNT OFF), Axin1 scaffolds NRF2 and GSK-3, facilitating NRF2 phosphorylation and further $\beta$-TrCP-dependent ubiquitination and proteasomal degradation. Under WNT-3A stimulation (WNT ON), Axin1 is recruited to the membrane, along with receptors LRP5/6 and Frizzled, and NRF2 is no longer phosphorylated by GSK-3. Then, NRF2 escapes $\beta$-TrCP-induced degradation, enters the nucleus, and dimerizes with MAF protein family members to transactivate ARE-containing genes, including, for example, those coding HO-1, NQO1, ME1, and G6PD. **(B)** Schematic interpretation of how WNT/Axin1 modulates zonation of the NRF2 signature. The concentration gradient of canonical WNT factors decreases from the perivenous to the periportal zones (49). Therefore, in normal livers, WNT signaling promotes NRF2 transcriptional activity to the first hepatocyte rows next to the CV. By contrast, Axin1 deficiency enhances NRF2 signature along the entire hepatic lobule. ME1, malic enzyme 1. To see this illustration in color, the reader is referred to the web version of this article at www.liebertpub.com/ars

experimental conditions has not yet been reported. In any case, the modest induction of NRF2 that escapes KEAP1 regulation has a physiological meaning. As an example, in pancreatic cancer, a modest K-Ras-dependent upregulation of less than two-fold in NRF2 transcription causes an increase in the NRF2 signature (9). Here, we extend the importance of modest increases in NRF2 to the modulation of antioxidant metabolism in the liver, and we propose that NRF2 levels appear to be fine-tuned not only by the relative levels of KEAP1 but also by other NRF2 interacting proteins which now include Axin1.

The molecular mechanisms responsible for maintenance of metabolic zonation in the liver are poorly understood. Oxygen gradients and hormones that run across the liver lobule participate in acquisition of periportal *versus* perivenous phenotypes of hepatocytes, and at least $\beta$-Catenin has been also involved in the upregulation of some antioxidant enzymes (2). The implication of NRF2 has not yet been studied, but very recently, it has been reported that $Nrf2^{-/-}$ mice develop a congenital intrahepatic shunt which alters hepatic oxygen and protein expression gradients (44). Here, by making use of liver-specific floxed $Axin1^{-/-}$ mice, we found a substantial increase in the transcriptional activity of NRF2 as determined by increased protein and mRNA levels of HO-1, NQO1, GCLM, ME1, and G6PDH. Moreover, compared with control livers, NRF2, HO-1, and NQO1 expression expanded to hepatocytes located beyond the initial rows of the hepatic central vein. In summary, these results indicate

that WNT signaling to NRF2 participates in maintenance of the perivenous hepatocyte phenotype. Figure 8B proposes a mechanism used by WNT/Axin1 to control zonation of NRF2 signature in the liver. It is interesting that other WNT-regulated transcription factors do not have this effect. Thus, c-MYC, a crucial element in APC-related tumorigenesis, does not seem to participate in liver zonation of ammonia detoxification (4). These facts suggest that Axin1 scaffolds several protein complexes with different functions.

It may seem somewhat intriguing that NRF2-mediated antioxidant metabolism is more noticeable in the perivenous zone, rather than in the periportal zone, which is more exposed to delivery of oxygen from the hepatic artery and xenobiotics from the portal vein. A possible explanation to this paradox is again the distinction between KEAP1-dependent regulation of NRF2, adapting NRF2 levels to transient demands, which should impact the periportal region, and the effect of WNT signaling that may be more related to the basal physiology of topologically different hepatocytes. There is evidence of basal low oxygen tension in the perivenous zone, with increased expression of hypoxia-inducible factor-$1\alpha$, $2\alpha$, and $3\alpha$ (23). Considering that hypoxia may lead to release of mitochondria-generated reactive oxygen species, a WNT-regulated developmental control of NRF2 might provide a KEAP1-independent layer of regulation to this zone.

The finding of an Axin1/NRF2 complex and its relevance in liver metabolism has important consequences for

therapy of liver diseases and probably others. Several pharmacological pipelines are being developed to inhibit WNT, particularly in cancer therapy (37). These drugs should be now tested for add-on effect on NRF2. On the other hand, WNT activators are also being considered and these should also provide a KEAP1-independent or complementary mechanism of NRF2 activation Here, we have used Axin1 stabilizers, acting as Tankyrase inhibitors (28), to inhibit NRF2 induction by WNT. Together, these studies open new therapeutic possibilities by targeting WNT/$\beta$-Catenin and, in our case, WNT/NRF2.

## Materials and Methods

### Cell culture and reagents

Hepatocytes from neonatal mice were obtained as previously reported (14) and grown in Dulbecco's modified Eagle's medium (DMEM) supplemented with 10% fetal bovine serum, 2 m$M$ L-glutamine, 20 m$M$ HEPES, and 80 $\mu$g/ml gentamycin. HEK293T cells were grown in DMEM supplemented with 10% fetal bovine serum and 80 $\mu$g/ml gentamycin. MEFs from $Keap1^{-/-}$ mice and $Keap1^{+/+}$ littermates were kindly provided by Dr. Ken Itoh (Center for Advanced Medical Research, Hirosaki University Graduate School of Medicine, Japan). Conditioned media from L-Control (Control-CM) and L-WNT-3A (WNT-3A-CM) confluent cells (grown in DMEM supplemented with 10% fetal bovine serum, 0.5 U/ml penicillin, and 0.5 $\mu$g/ml streptomycin) was collected and passed through a 0.2 $\mu$m filter. Transient transfections were performed with calcium phosphate, using reagents from Sigma-Aldrich, or with TransFectin™ lipid reagent from Bio-Rad. MG132, XAV939, and IWR-1 were from Sigma-Aldrich. Recombinant WNT-3A was from Cell Guidance Systems.

### Conditional Axin1 mutant mice

All animal experiments were performed according to UK Home Office regulations. Details of the generation of $Axin1^{-/-}$ mice are described in (10). Briefly, Ah-Cre mice were intercrossed with mice carrying LoxP-flanked Axin1 ($Axin1^{fl/fl}$) and Rosa 26 LacZ reporter alleles (LacZ) to generate $Axin1^{-/-}$ mice. Cre activity was induced by four intraperitoneal injections of $\beta$-naphthoflavone (BNF; 80 mg/kg body wt) over 4 days. Littermates were used as controls ($Axin1^{+/+}$). Three months after injections of BNF, the animals were sacrificed and liver samples were snap frozen in liquid nitrogen and stored at $-80$°C. For immunoblots, livers were homogenized in lysis buffer (50 m$M$ HEPES, 1% Triton X-100, 10 m$M$ EDTA, 50 m$M$ sodium pyrophosphate, 1 m$M$ phenylmethylsulfonyl fluoride, 0.1 $M$ sodium fluoride, 10 m$M$ sodium orthovanadate, and 1 $\mu$g/ml leupeptin) using the Brinkman PT 10/35 Polytron (American Laboratory Trading, Inc.). Extracts were kept ice cold at all times. Liver extracts were cleared by microcentrifugation at 40,000 $g$ (40 min, 4°C). The supernatants were aliquoted and stored at $-80$°C. For mRNA, livers were homogenized in TRIzol reagent using the Brinkman PT 10/35 Polytron.

### Plasmids

Expression vectors pcDNA3.1-mNRF2-V5/HisB and pcDNA3.1-mNRF2$^{\Delta ETGE}$-V5/HisB were provided by Dr. John D. Hayes (Biomedical Research Institute, Ninewells Hospital and Medical School, University of Dundee). pCGN-HA-GSK-3$\beta^{\Delta 9}$ was provided by Dr. Akira Kikuchi (Department of Biochemistry, Faculty of Medicine, Hiroshima University). pcDNA3-Flag-$\beta$-TrCP2 was provided by Dr. Tomoki Chiba (Department of Molecular Biology, University of Tsukuba). Plasmid encoding $\beta$-TrCP$^{\Delta Fbox}$ (pcDNA3-$\beta$-TrCP$^{\Delta Fbox}$-HA) was provided by Dr. Serge Y. Fuchs (Department of Animal Biology, University of Pennsylvania, Philadelphia, PA). Chimeric deletion constructs of the pEYFP-mNRF2-V5 were generated as described in (39, 40). pcDNA3.1-mNRF2$^{\Delta ETGE\ 6S/6A}$-V5/HisB was previously described in (38). Expression vector for WNT-3A (pCCBS-Hygro-WNT-3A-HA) was provided by Dr. Stuart A. Aaronson (Department of Oncological Sciences, Mount Sinai School of Medicine, New York, NY). Plasmid encoding mouse myc-Axin1 (pCMV5-myc-Axin1) was kindly provided by Dr. Sheng-Cai Lin (Department of Biochemistry, Hong Kong University of Science and Technology, Clear Water Bay, Kowloon, Hong Kong, China). Expression vectors for the myc-Axin1 deletion mutants were generated by polymerase chain reaction (PCR) using pCMV5-myc-Axin1 as a template with the following primers: Common forward, 5′ TAACGCGGCCGCAAGGT GGAAAAGGTGGACTGA 3′, reverse for myc-Axin1 (exons 2–5), 5′ TAACGCGGCCGCCCATGCGTACACGCTT CAGCC 3′, reverse for myc-Axin1 (2–6), 5′ TAACGCGG CCGCCACCAAAGGCCAAATCCCCAGC 3′, reverse for myc-Axin1 (2–7), 5′ TAACGCGGCCGCTCCCATGGCCT GCCTTCCGGTG 3′ and reverse for myc-Axin1 (2–8), 5′ TAACGCGGCCGCTCCTCTGCTTGGAGGGCAGTTT 3′ (NotI sites are underlined).

### Analysis of mRNA levels

Total RNA extraction, reverse transcription, and quantitative PCR were done as detailed in (39). See Supplementary Table S1 for primer sequences. Data analysis is based on the $\Delta\Delta Ct$ method with normalization of the raw data to housekeeping genes as described in the manufacturer's manual (Applied Biosystems). All PCRs were performed at least in triplicate.

### Immunoblotting

Immunoblots were performed as in (39). The primary antibodies are described in Supplementary Table S2. Proteins were detected by enhanced chemiluminescence (GE Healthcare).

### siRNA assays

siRNA used to knock down mouse NRF2, mouse $\beta$-TrCP1, mouse $\beta$-TrCP2, human GSK-3$\alpha$, human GSK3$\beta$ and mouse Axin1 expression, and control scrambled siRNA sequence are described in Supplementary Table S3. Immortalized hepatocytes were seeded in six-well plates (50,000 cells/well in 2 ml medium). When 40%–50% confluence was reached, cells were transfected with 25 nM siRNAs following DharmaFECT General Transfection Protocol (Dharmacon). After 48 h, cells were used for experiments. HEK293T cells were seeded in six-well plates (200,000 cells/well in 2 ml medium) before being transfected using calcium phosphate and the appropriate NRF2 expression plasmids. To knock down GSK-3 isoforms, we performed siRNA transfection during

two consecutive days. On the first day, we knocked down GSK-3 using 80 ng of Silencer Select validated siRNA with 30 $\mu$l of siPORT reagent, and on the second day we used 40 ng of Silencer Select validated siRNA with 15 $\mu$l of siPORT reagent. Twenty four hours later, the cells were collected and NRF2 and GSK-3 levels were analyzed. $Keap1^{-/-}$ MEFs were seeded in six-well plates (200,000 cells/well in 2 ml medium) at 16 h before transfection. To knock down Axin1, we performed siRNA transfection during two consecutive days. On the first day, we knocked down Axin1 using 50 or 100 pmol of Silencer Select validated siRNA with 20 $\mu$l of RNAimax Lipofectamine (Life Technologies), and on the second day we used 50 or 100 pmol of Silencer Select validated siRNA with 20 $\mu$l of RNAimax Lipofectamine. Twenty four hours later, the cells were harvested for analysis.

### Luciferase assays

Transient transfections of HEK293T or $Keap1^{-/-}$ cells were performed with the expression vectors ARE-LUC (a gift of Dr J. Alam, Department of Molecular Genetics, Ochsner Clinic Foundation, USA), or TOPFlash and FOPFlash, as indicated. pTK-Renilla were used as an internal control vector (Promega). Luciferase assays were performed as described in (39).

### In vivo ubiquitination assay

This was carried out using the method of Treier *et al.* (50). HEK293T cells were transfected with His-tagged Ubiquitin along with the indicated plasmids. Sixteen hours later, the transfected cells were washed with prewarmed phosphate-buffered saline and scraped into 0.4 ml of phosphate-buffered saline. Whole-cell lysates were prepared from 80 $\mu$l of the cell suspension and are referred to as the "input" fraction. His-tagged protein was purified from the remainder of the cell suspension as follows: The cell suspension was lysed by the addition to 1 ml of buffer A (6 $M$ guanidine:HCl, 10 m$M$ Tris in 0.1 $M$ phosphate buffer, pH 8.0) supplemented with 5 m$M$ imidazole. The resulting lysate was sonicated, to reduce viscosity. Then, 60 $\mu$l of Probond™ resin (Invitrogen) was added, and the mixture was rotated for 4 h at 25°C. Thereafter, the beads were washed sequentially with buffer A supplemented with 0.1% (v/v) Triton X-100, buffer B (8 $M$ urea, 10 m$M$ Tris in 0.1 $M$ phosphate buffer, pH 8.0) supplemented with 0.1% Triton X-100, buffer C (8 $M$ urea, 10 m$M$ Tris in 0.1 $M$ phosphate buffer, pH 6.5) supplemented with 0.2% Triton X-100, and finally, buffer C supplemented with 0.1% Triton X-100. Bound material was eluted from the beads by suspension in 50 $\mu$l of modified Laemmli sample buffer (20 m$M$ Tris-Cl, pH 6.8, 10% [v/v] glycerol, 0.8% [w/v] SDS, 0.1% [w/v] bromophenol blue, 0.72 $M$ 2-mercaptoethanol and 300 m$M$ imidazole) followed by boiling for 4 min. The suspension was centrifuged (16,000 $g$, 1 min, 20°C), and the resulting supernatant was collected and is referred to as the "pull down" fraction.

### Immunohistochemistry

Liver tissues from $Axin1^{+/+}$ and $Axin1^{-/-}$ mice were always dissected from the same part of the liver and fixed in ice-cold 10% neutral buffered formalin for no longer than 24 h before being processed into paraffin wax according to standard procedures. Tissue sections (5 $\mu$m thick) were used. The Streptavidin Biotin Peroxidase method was performed as follows: Sections were mounted on slides coated with 3-aminopropyltriethoxy-silane (Sigma Chemical Co.), hydrated after deparaffinization, and incubated for 10 min in 0.3% $H_2O_2$ in phosphate-buffered saline (PBS) to reduce endogenous peroxidase activity. For antigen retrieval, sections were submitted twice to microwave pretreatment for 2.5 min at 800 W in sodium citrate buffer 0.01 $M$ (pH 6) and subsequently blocked with Tris-buffered saline containing 1% bovine serum albumin. All sections were incubated for 16–20 h at 4°C with the primary antibody (diluted in PBS containing 1% serum albumin). Sections were washed in PBS to remove unbound primary antibodies and then incubated with a broad spectrum second antibody solution at room temperature. After incubations, the sections were washed and submitted to the supersensitive Streptavidin Biotin Peroxidase (Histostain-SP IHC kit, DAB sprectum, 95-9643; Life Technologies). The immunoreaction was developed by incubation with 3, 3-diaminobenzidine (DAB; Sigma-Aldrich) with $H_2O_2$ and diluted in phosphate buffer for peroxidase kits. The sections were counterstained with Harris' hematoxylin, dehydrated in ethanol, and mounted in DePex (Thermo Fisher Scientific). The primary antibodies and optimal dilutions used for these studies were as follows: anti-mouse NRF2 (1:50; generated in Cuadrado's laboratory), anti-GS (1:1000; Sigma-Aldrich), anti-HO-1 (1:50; Millipore), and anti-NQO1 (1:50; Abcam).

### Subcellular fractionation

$Keap1^{+/+}$ and $Keap1^{-/-}$ MEFs were seeded in p100 plates ($2 \times 10^6$ cells per plate). Cells were treated with Control or WNT-3A-CM for 4 h. Cytosolic and nuclear fractions were prepared as previously described (12). The supernatants from cytosolic and nuclear fractions were resolved in SDS-PAGE and immunoblotted with the indicated antibodies.

### Co-immunoprecipitation

Assays were performed as indicated in (39). The samples were resolved by SDS-PAGE and immunoblotted. Mouse IgG TrueBlot (eBiosciences) was used as peroxidase-conjugated secondary antibody (1:10,000 dilution) to avoid interference with the 55 kDa heavy and 23 kDa light chains of the immunoprecipitating antibody.

### Image analyses and statistics

Different band intensities (arbitrary units) corresponding to immunoblot detection of protein samples were quantified using the MCID software (MCID). Student's *t*-test, one-way, and two-way analysis of variance were used to assess differences between groups. Unless indicated, all experiments were performed at least thrice with similar results. The values in the graphs correspond to the mean of at least three samples. Results are expressed as mean ± SEM.

Histología y Neurociencia Facultad Medicina, UAM, Madrid) for technical assistance.

## Author Disclosure Statement

## References

 1. Abdullah A, Kitteringham NR, Jenkins RE, Goldring C, Higgins L, Yamamoto M, Hayes J, and Park BK. Analysis of the role of Nrf2 in the expression of liver proteins in mice using two-dimensional gel-based proteomics. *Pharmacol Rep* 64: 680–697, 2012.

 2. Benhamouche S, Decaens T, Godard C, Chambrey R, Rickman DS, Moinard C, Vasseur-Cognet M, Kuo CJ, Kahn A, Perret C, and Colnot S. Apc tumor suppressor gene is the "zonation-keeper" of mouse liver. *Dev Cell* 10: 759–770, 2006.

 3. Beyer TA, Xu W, Teupser D, auf dem Keller U, Bugnon P, Hildt E, Thiery J, Kan YW, and Werner S. Impaired liver regeneration in Nrf2 knockout mice: role of ROS-mediated insulin/IGF-1 resistance. *EMBO J* 27: 212–223, 2008.

 4. Burke ZD, Reed KR, Phesse TJ, Sansom OJ, Clarke AR, and Tosh D. Liver zonation occurs through a beta-catenin-dependent, c-Myc-independent mechanism. *Gastroenterology* 136: 2316–2324 e1–e3, 2009.

 5. Camp ND, James RG, Dawson DW, Yan F, Davison JM, Houck SA, Tang X, Zheng N, Major MB, and Moon RT. Wilms tumor gene on X chromosome (WTX) inhibits degradation of NRF2 protein through competitive binding to KEAP1 protein. *J Biol Chem* 287: 6539–6550, 2012.

 6. Chen B, Dodge ME, Tang W, Lu J, Ma Z, Fan CW, Wei S, Hao W, Kilgore J, Williams NS, Roth MG, Amatruda JF, Chen C, and Lum L. Small molecule-mediated disruption of Wnt-dependent signaling in tissue regeneration and cancer. *Nat Chem Biol* 5: 100–107, 2009.

 7. Chowdhry S, Zhang Y, McMahon M, Sutherland C, Cuadrado A, and Hayes JD. Nrf2 is controlled by two distinct beta-TrCP recognition motifs in its Neh6 domain, one of which can be modulated by GSK-3 activity. *Oncogene* 32: 3765–3781, 2013.

 8. Cullinan SB, Gordan JD, Jin J, Harper JW, and Diehl JA. The Keap1-BTB protein is an adaptor that bridges Nrf2 to a Cul3-based E3 ligase: oxidative stress sensing by a Cul3-Keap1 ligase. *Mol Cell Biol* 24: 8477–8486, 2004.

 9. DeNicola GM, Karreth FA, Humpton TJ, Gopinathan A, Wei C, Frese K, Mangal D, Yu KH, Yeo CJ, Calhoun ES, Scrimieri F, Winter JM, Hruban RH, Iacobuzio-Donahue C, Kern SE, Blair IA, and Tuveson DA. Oncogene-induced Nrf2 transcription promotes ROS detoxification and tumorigenesis. *Nature* 475: 106–109, 2011.

10. Feng GJ, Cotta W, Wei XQ, Poetz O, Evans R, Jarde T, Reed K, Meniel V, Williams GT, Clarke AR, and Dale TC. Conditional disruption of Axin1 leads to development of liver tumors in mice. *Gastroenterology* 143: 1650–1659, 2012.

11. Gao C, Xiao G, and Hu J. Regulation of Wnt/beta-catenin signaling by posttranslational modifications. *Cell Biosci* 4: 13, 2014.

12. Garcia-Yague AJ, Rada P, Rojo AI, Lastres-Becker I, and Cuadrado A. Nuclear import and export signals control the subcellular localization of Nurr1 protein in response to oxidative stress. *J Biol Chem* 288: 5506–5517, 2013.

13. Gebhardt R and Hovhannisyan A. Organ patterning in the adult stage: the role of Wnt/beta-catenin signaling in liver zonation and beyond. *Dev Dyn* 239: 45–55, 2010.

14. Gonzalez-Rodriguez A, Clampit JE, Escribano O, Benito M, Rondinone CM, and Valverde AM. Developmental switch from prolonged insulin action to increased insulin sensitivity in protein tyrosine phosphatase 1B-deficient hepatocytes. *Endocrinology* 148: 594–608, 2007.

15. Hayes JD and Dinkova-Kostova AT. The Nrf2 regulatory network provides an interface between redox and intermediary metabolism. *Trends Biochem Sci* 39: 199–218, 2014.

16. Higgins LG and Hayes JD. The cap'n'collar transcription factor Nrf2 mediates both intrinsic resistance to environmental stressors and an adaptive response elicited by chemopreventive agents that determines susceptibility to electrophilic xenobiotics. *Chem Biol Interact* 192: 37–45, 2011.

17. Hu M, Zou Y, Nambiar SM, Lee J, Yang Y, and Dai G. Keap1 modulates the redox cycle and hepatocyte cell cycle in regenerating liver. *Cell Cycle* 13: 2349–2358, 2014.

18. Hu R, Xu C, Shen G, Jain MR, Khor TO, Gopalkrishnan A, Lin W, Reddy B, Chan JY, and Kong AN. Gene expression profiles induced by cancer chemopreventive isothiocyanate sulforaphane in the liver of C57BL/6J mice and C57BL/6J/Nrf2 (−/−) mice. *Cancer Lett* 243: 170–192, 2006.

19. Huang SM, Mishina YM, Liu S, Cheung A, Stegmeier F, Michaud GA, Charlat O, Wiellette E, Zhang Y, Wiessner S, Hild M, Shi X, Wilson CJ, Mickanin C, Myer V, Fazal A, Tomlinson R, Serluca F, Shao W, Cheng H, Shultz M, Rau C, Schirle M, Schlegl J, Ghidelli S, Fawell S, Lu C, Curtis D, Kirschner MW, Lengauer C, Finan PM, Tallarico JA, Bouwmeester T, Porter JA, Bauer A, and Cong F. Tankyrase inhibition stabilizes axin and antagonizes Wnt signalling. *Nature* 461: 614–620, 2009.

20. Itoh K, Mimura J, and Yamamoto M. Discovery of the negative regulator of Nrf2, Keap1: a historical overview. *Antioxid Redox Signal* 13: 1665–1678, 2010.

21. Jungermann K and Kietzmann T. Zonation of parenchymal and nonparenchymal metabolism in liver. *Annu Rev Nutr* 16: 179–203, 1996.

22. Kajla S, Mondol AS, Nagasawa A, Zhang Y, Kato M, Matsuno K, Yabe-Nishimura C, and Kamata T. A crucial role for Nox 1 in redox-dependent regulation of Wnt-beta-catenin signaling. *FASEB J* 26: 2049–2059, 2012.

23. Kietzmann T, Cornesse Y, Brechtel K, Modaressi S, and Jungermann K. Perivenous expression of the mRNA of the three hypoxia-inducible factor alpha-subunits, HIF1alpha, HIF2alpha and HIF3alpha, in rat liver. *Biochem J* 354: 531–537, 2001.

24. Kitteringham NR, Abdullah A, Walsh J, Randle L, Jenkins RE, Sison R, Goldring CE, Powell H, Sanderson C, Williams S, Higgins L, Yamamoto M, Hayes J, and Park BK. Proteomic analysis of Nrf2 deficient transgenic mice reveals cellular defence and lipid metabolism as primary Nrf2-dependent pathways in the liver. *J Proteomics* 73: 1612–1631, 2010.

25. Klaassen CD and Reisman SA. Nrf2 the rescue: effects of the antioxidative/electrophilic response on the liver. *Toxicol Appl Pharmacol* 244: 57–65, 2010.

26. Kobayashi A, Kang MI, Okawa H, Ohtsuji M, Zenke Y, Chiba T, Igarashi K, and Yamamoto M. Oxidative stress sensor Keap1 functions as an adaptor for Cul3-based E3

ligase to regulate proteasomal degradation of Nrf2. *Mol Cell Biol* 24: 7130–7139, 2004.

27. Kohler UA, Kurinna S, Schwitter D, Marti A, Schafer M, Hellerbrand C, Speicher T, and Werner S. Activated Nrf2 impairs liver regeneration in mice by activation of genes involved in cell-cycle control and apoptosis. *Hepatology* 60: 670–678, 2014.

28. Lehtio L, Chi NW, and Krauss S. Tankyrases as drug targets. *FEBS J* 280: 3576–3593, 2013.

29. Li VS, Ng SS, Boersema PJ, Low TY, Karthaus WR, Gerlach JP, Mohammed S, Heck AJ, Maurice MM, Mahmoudi T, and Clevers H. Wnt signaling through inhibition of beta-catenin degradation in an intact Axin1 complex. *Cell* 149: 1245–1256, 2012.

30. McMahon M, Itoh K, Yamamoto M, and Hayes JD. Keap1-dependent proteasomal degradation of transcription factor Nrf2 contributes to the negative regulation of antioxidant response element-driven gene expression. *J Biol Chem* 278: 21592–21600, 2003.

31. McMahon M, Thomas N, Itoh K, Yamamoto M, and Hayes JD. Dimerization of substrate adaptors can facilitate cullin-mediated ubiquitylation of proteins by a ''tethering'' mechanism: a two-site interaction model for the Nrf2-Keap1 complex. *J Biol Chem* 281: 24756–24768, 2006.

32. Mitsuishi Y, Taguchi K, Kawatani Y, Shibata T, Nukiwa T, Aburatani H, Yamamoto M, and Motohashi H. Nrf2 redirects glucose and glutamine into anabolic pathways in metabolic reprogramming. *Cancer Cell* 22: 66–79, 2012.

33. Mobasher MA, Gonzalez-Rodriguez A, Santamaria B, Ramos S, Martin MA, Goya L, Rada P, Letzig L, James LP, Cuadrado A, Martin-Perez J, Simpson KJ, Muntane J, and Valverde AM. Protein tyrosine phosphatase 1B modulates GSK3beta/Nrf2 and IGFIR signaling pathways in acetaminophen-induced hepatotoxicity. *Cell Death Dis* 4: e626, 2013.

34. Monga SP. Role and regulation of beta-catenin signaling during physiological liver growth. *Gene Expr* 16: 51–62, 2014.

35. Nejak-Bowen K and Monga SP. Wnt/beta-catenin signaling in hepatic organogenesis. *Organogenesis* 4: 92–99, 2008.

36. Noutsou M, Duarte AM, Anvarian Z, Didenko T, Minde DP, Kuper I, de Ridder I, Oikonomou C, Friedler A, Boelens R, Rudiger SG, and Maurice MM. Critical scaffolding regions of the tumor suppressor Axin1 are natively unfolded. *J Mol Biol* 405: 773–786, 2011.

37. Pez F, Lopez A, Kim M, Wands JR, Caron de Fromentel C, and Merle P. Wnt signaling and hepatocarcinogenesis: molecular targets for the development of innovative anticancer drugs. *J Hepatol* 59: 1107–1117, 2013.

38. Rada P, Rojo AI, Chowdhry S, McMahon M, Hayes JD, and Cuadrado A. SCF/{beta}-TrCP promotes glycogen synthase kinase 3-dependent degradation of the Nrf2 transcription factor in a Keap1-independent manner. *Mol Cell Biol* 31: 1121–1133, 2011.

39. Rada P, Rojo AI, Evrard-Todeschi N, Innamorato NG, Cotte A, Jaworski T, Tobon-Velasco JC, Devijver H, Garcia-Mayoral MF, Van Leuven F, Hayes JD, Bertho G, and Cuadrado A. Structural and functional characterization of Nrf2 degradation by the glycogen synthase kinase 3/beta-TrCP axis. *Mol Cell Biol* 32: 3486–3499, 2012.

40. Rojo AI, Rada P, Egea J, Rosa AO, Lopez MG, and Cuadrado A. Functional interference between glycogen synthase kinase-3 beta and the transcription factor Nrf2 in

protection against kainate-induced hippocampal cell death. *Mol Cell Neurosci* 39: 125–132, 2008.

41. Rojo AI, Rada P, Mendiola M, Ortega-Molina A, Wojdyla K, Rogowska-Wresinska A, Hardisson D, Serrano M, and Cuadrado A. The PTEN/NRF2 axis promotes human carcinogenesis. *Antioxid Redox Signal* 21: 2498–2514, 2014.

42. Shin SM, Yang JH, and Ki SH. Role of the Nrf2-ARE pathway in liver diseases. *Oxid Med Cell Longev* 2013: 763257, 2013.

43. Shirasaki K, Taguchi K, Unno M, Motohashi H, and Yamamoto M. NF-E2-related factor 2 promotes compensatory liver hypertrophy after portal vein branch ligation in mice. *Hepatology* 59: 2371–2382, 2014.

44. Skoko JJ, Wakabayashi N, Noda K, Kimura S, Tobita K, Shigemura N, Tsujita T, Yamamoto M, and Kensler TW. Loss of Nrf2 in mice evokes a congenital intrahepatic shunt that alters hepatic oxygen and protein expression gradients and toxicity. *Toxicol Sci* 141: 112–119, 2014.

45. Stamos JL and Weis WI. The beta-catenin destruction complex. *Cold Spring Harb Perspect Biol* 5: a007898, 2013.

46. Taguchi K, Hirano I, Itoh T, Tanaka M, Miyajima A, Suzuki A, Motohashi H, and Yamamoto M. Nrf2 enhances cholangiocyte expansion in Pten-deficient livers. *Mol Cell Biol* 34: 900–913, 2014.

47. Taguchi K, Maher JM, Suzuki T, Kawatani Y, Motohashi H, and Yamamoto M. Genetic analysis of cytoprotective functions supported by graded expression of Keap1. *Mol Cell Biol* 30: 3016–3026, 2010.

48. Tong KI, Kobayashi A, Katsuoka F, and Yamamoto M. Two-site substrate recognition model for the Keap1-Nrf2 system: a hinge and latch mechanism. *Biol Chem* 387: 1311–1320, 2006.

49. Torre C, Perret C, and Colnot S. Molecular determinants of liver zonation. *Prog Mol Biol Transl Sci* 97: 127–150, 2010.

50. Treier M, Staszewski LM, and Bohmann D. Ubiquitin-dependent c-Jun degradation *in vivo* is mediated by the delta domain. *Cell* 78: 787–798, 1994.

51. Villeneuve NF, Lau A, and Zhang DD. Regulation of the Nrf2-Keap1 antioxidant response by the ubiquitin proteasome system: an insight into cullin-ring ubiquitin ligases. *Antioxid Redox Signal* 13: 1699–1712, 2010.

52. Wakabayashi N, Shin S, Slocum SL, Agoston ES, Wakabayashi J, Kwak MK, Misra V, Biswal S, Yamamoto M, and Kensler TW. Regulation of notch1 signaling by nrf2: implications for tissue regeneration. *Sci Signal* 3: ra52, 2010.

53. Wang X, Tomso DJ, Chorley BN, Cho HY, Cheung VG, Kleeberger SR, and Bell DA. Identification of polymorphic antioxidant response elements in the human genome. *Hum Mol Genet* 16: 1188–1200, 2007.

54. Wu K, Fuchs SY, Chen A, Tan P, Gomez C, Ronai Z, and Pan ZQ. The SCF(HOS/beta-TRCP)-ROC1 E3 ubiquitin ligase utilizes two distinct domains within CUL1 for substrate targeting and ubiquitin ligation. *Mol Cell Biol* 20: 1382–1393, 2000.

55. Wu KC, Cui JY, and Klaassen CD. Effect of graded Nrf2 activation on phase-I and -II drug metabolizing enzymes and transporters in mouse liver. *PLoS One* 7: e39006, 2012.

56. Zhang DD, Lo SC, Cross JV, Templeton DJ, and Hannink M. Keap1 is a redox-regulated substrate adaptor protein for a Cul3-dependent ubiquitin ligase complex. *Mol Cell Biol* 24: 10941–10953, 2004.

57. Zhang YK, Wu KC, and Klaassen CD. Genetic activation of Nrf2 protects against fasting-induced oxidative stress in livers of mice. *PLoS One* 8: e59122, 2013.

Address correspondence to:
*Dr. Antonio Cuadrado*
*Instituto de Investigaciones Biomédicas*
*''Alberto Sols'' UAM-CSIC*
*C/Arturo Duperier 4*
*Madrid 28029*
*Spain*

*E-mail:* antonio.cuadrado@uam.es

---

### Abbreviations Used

$\beta$-TrCP = beta-transducin repeat containing protein
ANOVA = analysis of variance
ARE = antioxidant response element
DMEM = Dulbecco's modified Eagle's medium
EYFP = enhanced yellow fluorescent protein
G6PDH = glucose 6 phosphate dehydrogenase
Gclc = $\gamma$-glutamyl cysteine ligase catalytic subunit
Gclm = $\gamma$-glutamyl cysteine ligase modulator subunit
CM = conditioned medium
Gpx1 = glutathione peroxidase 1

---

ME1 = malic enzyme 1
Nqo1 = NAD(P)H:quinone oxidoreductase 1
GS = glutamine synthetase
GSK-3 = glycogen synthase kinase-3
HEK293T = human embryonic kidney cells expressing the T antigen
Hmox1 = gene encoding heme oxigenase-1
HO-1 = heme oxygenase-1
IHC = immunohistochemistry
KEAP1 = Kelch-like ECH-associated protein 1
Me1 = malic enzyme
MEFs = mouse embryonic fibroblasts
NFE2L2 = nuclear factor (erythroid-derived 2)-like 2
NOX1 = NADPH oxidase 1
NRF2 = nuclear factor (erythroid-derived 2)-like 2
PCR = polymerase chain reaction
PTEN = phosphatase and tensin homolog
qRT-PCR = quantitative real time PCR
Rbx1 = ring-box 1
SCF = Skp, Cullin, and F-box containing complex
siRNA = short interfering RNA
TCF/LEF = T-cell factor/lymphoid enhancer factor
WB = Western blot
WNT = wingless-type protein
WTX = Wilms tumor gene on X chromosome